Icarus 226 (2013) 999–1019

Contents lists available at ScienceDirect

Icarus

journal homepage: www.elsevier.com/locate/icarus

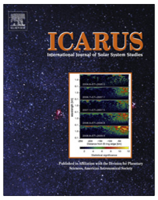

The inner small satellites of Saturn: A variety of worlds

P.C. Thomas [a,*], J.A. Burns [a], M. Hedman [a], P. Helfenstein [a], S. Morrison [b], M.S. Tiscareno [a], J. Veverka [a]

[a] *Center for Radiophysics and Space Research, Cornell University, Ithaca, NY 14853, USA*
[b] *Department of Planetary Sciences, University of Arizona, Tucson, AZ 85721, USA*

ARTICLE INFO

Article history:
Received 22 March 2013
Revised 10 July 2013
Accepted 13 July 2013
Available online 22 July 2013

Keywords:
Saturn, Satellites
Geological processes
Geophysics
Photometry

ABSTRACT

More than a dozen small (<150 km mean radius) satellites occupy distinct dynamical positions extending from within Saturn's classical rings to the orbit of Dione. The Cassini mission has gradually accumulated image and spectral coverage of these objects to the point where some generalizations on surface morphology may be made. Objects in different dynamical niches have different surface morphologies. Satellites within the main rings display equatorial ridges. The F-ring shepherding satellites show structural forms and heavily cratered surfaces. The co-orbitals Janus and Epimetheus are the most lunar-like of the small satellites. Satellites occupying libration zones (Trojan satellites) have deep covering of debris subject to downslope transport. Small satellites embedded in ring arcs are distinctively smooth ellipsoids that are unique among small, well-observed Solar System bodies and are probably relaxed, effectively fluid equilibrium shapes indicative of mean densities of about 300 kg m^{-3}.

1. Introduction

The smaller (<150 km mean radius) satellites of Saturn occupy several dynamical niches: associated with rings (Pan, Daphnis, Atlas, Prometheus, Pandora), co-orbiting between the F ring and the larger satellites (Janus and Epimetheus), orbiting in faint rings or in ring arcs (Aegaeon, Methone, Anthe, Pallene), and orbiting libration points of larger moons (Telesto, Calypso, Polydeuces, and Helene). Hyperion, the largest irregularly-shaped satellite of Saturn, orbits between Titan and Iapetus, and Phoebe, the next largest, is in a retrograde orbit well outside the orbits of the large satellites. Many smaller objects orbit farther from Saturn (Gladman et al., 2001; Denk et al., 2011); they are not resolved in Cassini images and are not considered in this work.

The small satellites do not experience the internally driven processes that larger objects do, but the imaging survey by Cassini has shown distinct differences in morphology among the small objects that vary with their orbital and dynamical groupings. This correlation suggests that their morphologies, shaped by external rather than internal processes, may reveal aspects of the dynamics of materials orbiting close to Saturn. This work examines the morphological characteristics of these satellites and outlines some of the possible mechanisms that may explain the variations among objects that do not suffer effects of internal activity.

The small satellites generally are expected to be fragments or rubble-like assemblages. The higher-density example of Phoebe may be an exception (Johnson et al., 2009; Castillo-Rogez et al., 2012) as its shape suggests an early relaxation to a nearly spherical object, possibly the result of internal heating. Nearly all of these objects have been imaged by Cassini at pixel scales of <300 m (Table S1), although not over their entire surfaces. These resolutions allow comparison of shapes, surface features, photometry, and colors. The basic shapes, densities, and some surface features of the small saturnian satellites have been discussed in Porco et al. (2005) (Phoebe), Porco et al. (2007) (ring satellites), and Thomas (2010). With the exception of Phoebe, all of these objects that have measured masses appear to have mean densities consistent with highly porous water ice. Other components are almost certainly present, but likely constitute onlysmall amounts (Filacchione et al., 2010; Buratti et al., 2010). Model porosities assuming a solid density of 930 kg m^{-3} (appropriate for water ice) are ~30–60%. Addition of a denser component would increase these model porosities.

This paper uses Cassini Imaging Science Subsystem (ISS; Porco et al., 2004) data obtained through mid-2012 to update the shapes and characteristics of these small satellites. Notably better data will not be obtained until 2015. We deal with all the inner groupings of the small saturnian satellites, but concentrate on the ring-arc embedded satellites and on the Trojan satellites co-orbiting with Tethys and Dione.

2. Data and methods

All images used are from the Cassini Imaging Science Subsystem (Owen, 2003; Porco et al., 2004); most are from the Narrow Angle Camera (NAC) which has a pixel scale of 6 km at a million km range. Shape models of the satellites have been gradually improved

---

* Corresponding author.
E-mail address: pct2@cornell.edu (P.C. Thomas).

0019-1035/$ - see front matter © 2013 Elsevier Inc. All rights reserved.
http://dx.doi.org/10.1016/j.icarus.2013.07.022

with data from multiple flybys at a variety of resolutions, viewing angles, and phase angles. The orbit of the Cassini spacecraft has changed during the mission to support different goals, some of which require high inclinations that lead to periods of months or years between close imaging of small satellites.

Stereo control point solutions are the basis of the shape models and libration studies. Control points are marked manually on images covering as wide a range of observer geometries as possible with the POINTS program (J. Joseph; in Thomas et al. (2002)Thomas et al. (2002)). Some additional control points have been added through automated image matching, but these are a small minority of the points that are used. Resolutions of the images used vary greatly due to the nature of the different flyby trajectories. Residuals of the control point solutions (predicted vs. observed image locations) are typically 0.3–0.4 pixels. Shape models are fit to the stereo points, and modified based on limb profiles. The shape models are derived in the form of latitude, longitude, radius at 2° intervals in latitude and longitude (Simonelli et al., 1993) but for some purposes can be converted to more evenly spaced x, y, z triangular plate models. In some cases Saturn-shine or silhouettes of the satellites in front of Saturn provide crucial coverage of limbs or of control points. Description of the techniques are in Simonelli et al. (1993) and Thomas et al. (2007a).

Solving for the control points requires knowledge of the instantaneous orientation of the object. Correctly predicting the satellites' orientations requires accurate orbital and rotational data, including information on any forced libration (Tiscareno et al., 2009). Our model for Helene's orientation is of the same form as that described by Tiscareno et al., based on the moon maintaining synchronous rotation (even as the orbit frequency changes due to the co-orbital resonance) with additional librations of variable amplitude that track the instantaneous orbit frequency. More detailed dynamical analysis (Noyelles, 2010; Robutel et al., 2011a) confirmed in the case of Janus and Epimetheus that there are no observable deviations from the Tiscareno et al. model, as expected for a moon whose rotational dynamics are dominated by in-plane forced librations due to its non-spherical shape. Although Robutel et al. (2011b) recently presented a detailed dynamical analysis of the orientation of Helene, we choose for this work to continue using the Tiscareno et al. model, which gives sufficient precision, is easy to implement, and is physically intuitive. The control-point solutions for Helene suggest any forced libration is <1° (Fig. S3). Predictions on possible forced librations based on the shape model alone are limited both by necessary assumptions of a homogeneous interior as well as low-resolution views of some longitudes, and the presence of an as-yet unimaged region including the north pole. The model moment ratio from the current shape model for $(B-A)/C$ is 0.014, which would predict physical librations of <0.1°, a value we are far from being able to detect.

For Calypso and Telesto, we obtained sufficiently precise control point results from a model assuming a constant rotation rate, as any librations were undetectable probably due to their smaller amplitudes of libration in the co-orbital resonance (Oberti and Vienne, 2003; Murray et al., 2005).

For the more ellipsoidal objects, shapes are determined by measurement of limb coordinates for an analytical ellipsoidal fit. Scans are taken in images along line or sample directions and the position of a sharp bright edge is modeled in steps of 0.05 pixels; the limb coordinate is selected as the best match of predicted and observed brightness. The line and sample coordinates so obtained are corrected for spacecraft range and optical distortion to relative positions in km in the viewing plane. An ellipsoid is then fit to views from different directions, allowing the three ellipsoidal axes and the coordinate center to vary. The uncertainties in range and orientation of the image are assumed to induce errors in the shape that are small compared to other sources of error; see Dermott and Thomas (1988) for a discussion of the effects of such errors on the solutions. Precision of the limb measurement is commonly better than 0.1 pixel. The uncertainty in ellipsoidal solutions depends on the limb topography (roughness, or how close to an ellipsoid it is), resolution, and the spread of viewpoints that constrain the solution.

Crater counting and feature mapping are done interactively with the POINTS program. Features are mapped using manually stretched images. Locations of mapped points are the projection of single points, or centers of ellipses (such as crater rims) on the shape model in particular images. Data are stored in text files that include body-centered and image locations, and image and lighting information. Past experience in mapping irregular objects shows that crater counts are reliable down to diameters of 5–7 pixels and in images above 45° phase. Mapping coordinates use West longitudes, per the IAU rules for satellites (Archinal et al., 2011), and 0°W is on the (on average) sub-Saturn point. Topography is described by dynamic heights (H_d; Vanicek and Krakiwsky, 1986; Thomas, 1993) which are similar to, but not identical with, heights above an equipotential. H_d is the potential energy at a point on the surface divided by an average surface acceleration. The potential energy calculation accounts for the irregular shape of the body's mass assuming uniform density, and rotational and tidal accelerations.

For our photometric work we first radiometrically calibrated the ISS images with the CISSCAL computer program, which is available through the Planetary Data System (PDS). Details of the ISS Camera calibration are given in West et al. (2010), Porco et al. (2004), and the CISSCAL User's Manual (http://pds-rings.seti.org/cassini/iss/software.html). In the calibrated images, pixel DN values are scaled to radiance factors, $I/\mathcal{F}$, where I is the specific scattered intensity of light and $\pi\mathcal{F}$ is the specific plane-parallel solar flux over the wavelength range of the filter bandpass. We rely on the four ISS NAC multispectral filters that were most frequently used during close-flybys as well as distant imaging of the satellites; CL1–CL2 (611 nm), CL1–UV3 (338 nm), CL1–GRN (568 nm), and CL1–IR3 (930 nm). Sampling of whole-disk and disk-resolved photometric measurements follows the approach of Helfenstein et al. (1994). In general, disk-resolved measurements were obtained only from images for which the diameter of the object in pixels was larger than 100 pixels. Local angles of incidence (i), emission (e), and phase angle (α) on the surfaces of the satellites were obtained using the appropriate satellite shape model and corrected camera pointing geometry via the POINTS program, cited earlier. From each image, the pixel-by-pixel disk-resolved radiance factors were measured and binned into 10° increments of photometric latitude and longitude.

3. Ring satellites

3.1. Pan, Atlas, Daphnis

These objects have been studied previously by Porco et al. (2007) and Charnoz et al. (2007). Pan (mean radius R_m, of 14 km) within the Encke gap of Saturn's A ring, and Atlas (R_m = 15 km), just outside the A ring, have been imaged at sufficient resolution to show distinct equatorial ridges giving these somewhat elongated objects "flying saucer"-like shapes. (Fig. 1, Table 1). Daphnis (R_m = 3.8 km) is also elongate and although it is less well-resolved than Pan and Atlas in terms of pixels/radius, it does have low-latitude ridge and is also somewhat saucer-shaped in that the a and b axes are both fractionally much larger than the c axis. These three objects rotate at least approximately synchronously with their orbital periods; synchroneity must be estimated by congruence of shape models at scattered, low-resolution views. Atlas is within